# Electronic Properties of 4-Substituted Naphthalimides

**Pavel Kucheryavy,[†] Guifeng Li,[†] Shubham Vyas,[‡] Christopher Hadad,[‡] and Ksenija D. Glusac*[,†]**

*Department of Chemistry, Bowling Green State University, Bowling Green, Ohio 43403, and Department of Chemistry, Ohio State University, 100 West 18th Avenue, Columbus, Ohio 43210*

*Received: March 4, 2009; Revised Manuscript Received: April 27, 2009*

This paper describes a study of excited-state properties of naphthalimide (NI) and four 4-substituted derivatives: 4-chloronaphthalimide (Cl-NI), 4-methylthionaphthalimide (MeS-NI), 4-nitronaphthalimide ($O_2$N-NI), and 4-(*N*,*N*-dimethylaminonaphthalimide ($Me_2$N-NI). Steady-state absorption and fluorescence spectra were collected in solvents of varying polarity to determine the excited-state character of NI derivatives. Furthermore, the excited-state dynamics were studied using femtosecond transient absorption spectroscopy. The experimental findings were compared to calculated data obtained using time-dependent density functional (TD-DFT) methods. We found that light absorption by all NI derivatives leads to the production of the second excited state ($S_2$), which was found to have a n,$\pi$* character. Within ~40 ps, the $S_2$ state undergoes internal conversion to produce the $S_1$ state. The $S_1$ state is relatively long-lived (~4 ns) and has charge-transfer character in NI derivatives with electron-withdrawing and electron-donating groups (MeS-NI, $O_2$N-NI, and $Me_2$N-NI). In the case of NI and Cl-NI, the $S_1$ state has a $\pi$,$\pi$* character and undergoes intersystem crossing to produce the $T_1$ state within 400 ps.

## Introduction

Naphthalimides (NIs) belong to a class of chromophores for which excited-state properties can be drastically changed by the nature of a substituent present on the aromatic ring.[1−3] While the nonpolar $\pi$,$\pi$* state occurs in the parent NI (i.e., without any substituents at the 4-position), the introduction of electron-donating or -withdrawing substituents (amino or nitro groups) induces a polar charge-transfer (CT) excited state.[3] The compounds with CT character are especially interesting due to their strong oxidizing or reducing capacity. The oxidative nature of NIs, coupled with their ability to intercalate DNA bases, has been used in DNA photocleavage reactions.[1] The oxidative cleavage of DNA has been demonstrated to be site-specific, with the damage occurring at the 5′ site of the most electron-rich GG site.[2] In addition, it was found that the cleavage location can be changed from the GG to the T site by simply using nitro derivatives of NI.[2] The reason for the change in the reactivity was assigned to H-atom abstraction from the methyl group of thymine by the nitro group of NI. DNA cleavage has also been accomplished indirectly, by *N*-hydroperoxy derivatives of NI, which produce OH radicals that in turn damage DNA.[4] The capability of NIs to induce light-triggered DNA damage has been used in photodynamic therapy to destroy HIV blood viruses.[5] In addition to the reactivity toward nucleic acids, NIs have been found to induce photocross-linking of proteins,[6] which has been applied in light-induced tissue repair.[7]

The CT characteristics of NI excited states have also found use in organic materials, such as donor−acceptor systems for solar cells,[8] organic light-emitting diodes (oLEDs),[9] and sensors for metal ions and protons.[10−12] In oLEDs, the advantage of 4-substituted NIs is in their low reduction potential and wide energy gaps, along with the high fluorescence efficiency. Emission from intramolecular CT states contributes greatly to the electroluminescence of these devices. In the design of materials for solar cells, NIs are commonly used either as electron donors or as acceptors in D−A chemical systems designed for long-lived charge separation.[8] In sensor applications, the molecular system is generally constructed from NI with an alkyl-amino substituent. The amino group is involved in photoinduced electron transfer, which diminishes the fluorescence lifetime. However, if metal ions or protons are present in the solution, the fluorescence of the NI unit is restored, leading to a "turn-on" sensing.

Because of these light-triggered applications of NI derivatives, many groups have studied their excited-state behavior.[13−15] All of the compounds studied thus far contain substituents at the imide nitrogen of the NI framework. We are interested in using NIs as parts of hydrogen-bonded donor−acceptor systems that are capable of producing long-lived charge separation due to a proton-coupled electron transfer process. For this purpose, NIs offer several great advantages: (i) They absorb strongly in the UV/vis region, (ii) the oxidation and reduction potential of NIs can be readily tuned by substitution, and (iii) the imide moiety of NIs is capable of making hydrogen bonds with the acceptor. For these reasons, we sought to investigate the excited-state properties of NIs that lack any substituents in the imide position.

In this paper, we present a detailed study of the electronic properties of NI and 4-substituted derivatives shown in Scheme 1. We varied the nature of the substituents from electron-donating (MeS-NI and $Me_2$N-NI) to electron-withdrawing (6-nitrobenzo[de]isoquinoline-1,3-dione, $O_2$N-NI). We present the solvent-dependent steady-state absorption and fluorescence data, femtosecond optical transient absorption data, and density functional theory (DFT) calculations of NI derivatives in their ground and excited states. In contrast to previous reports,[16] we find that the excitation of NI derivatives creates an n,$\pi$* excited state. In the case of NI and 4-chloro-1,8-naphthalimide (Cl-NI), the n,$\pi$* state is also responsible for their fluorescence.

* To whom correspondence should be addressed. E-mail: kglusac@bgsu.edu.
[†] Bowling Green State University.
[‡] Ohio State University.

10.1021/jp901982r CCC: $40.75 
Published on Web 05/15/2009

**SCHEME 1: Structures of Napthalimide and 4-Substituted Derivatives**

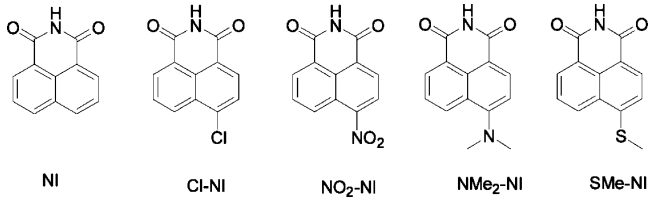


**SCHEME 2: Synthetic Procedure for the Preparation of $NMe_2$-NI and SMe-NI**

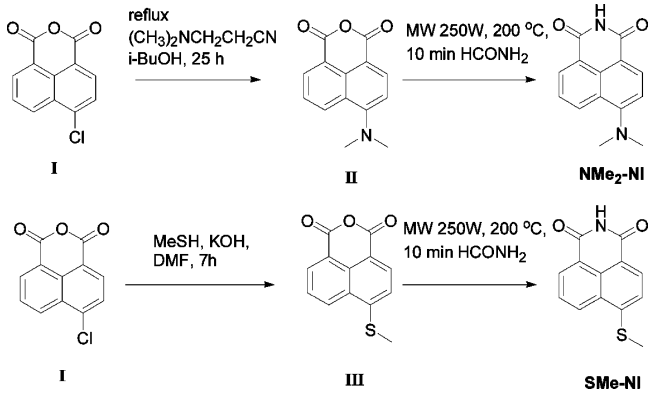


On the other hand, $Me_2N$-NI, MeS-NI, and $O_2N$-NI seem to have different states involved in the absorption and emission spectra. In these derivatives, the initial absorption creates an n,$\pi^*$ excited state, which within 40 ps undergoes an internal conversion to the polar CT $\pi,\pi^*$ state. Furthermore, we find that in polar solvents, $Me_2N$-NI undergoes an excited-state conformational change to produce a twisted-intermolecular CT state.

## Experimental Section

**Materials.** Dioxane (99% ACS reagent grade), acetonitrile [high-performance liquid chromatography (HPLC) grade], and dimethyl sulfoxide (DMSO, spectrophotometric grade) were purchased from Aldrich. Chloroform (HPLC grade) and dichloromethane (HPLC grade) were ordered from EMD. 2-Butanone (spectrophotometric grade) was obtained from Acros Organics, while acetone (for UV spectroscopy) and fluorobenzene (for UV spectroscopy) were obtained from Fluka. Acetone, chloroform, and dichloromethane were distilled before use. 1,8-Naphtalimide (NI) was purchased from Aldrich. Cl-NI was purchased from ChemPacific. $O_2N$-NI was obtained from TimTech library. Compound **I** (6-chlorobenzo[de]isochromene-1,3-dione, Scheme 2), 3-(*N*,*N*-dimethylamino)propionitrile, and methanethiol were purchased from Aldrich. All of these chemicals were used as received.

**Synthesis.** Compounds were identified using $^1$H NMR and $^{13}$C NMR, in DMSO-$d_6$ (Aldrich) on a Bruker 300 MHz spectrometer at room temperature. Gas chromatography−mass spectrometry (GC-MS) analysis was performed using Shimadzu QP5050A equipment. Compound **II** was synthesized using the published procedure.[17]

**Compound III (6-Methylsulfanylbenzo[de]isochromene-1,3-dione).** Compound **I** (1 g) and sodium hydroxide (0.5 g) were dissolved in 20 mL of dimethyl formamide (DMF). Methanethiol was initially condensed (~2 mL) in a trap placed in dry ice. All of the methanethiol was purged through the mixture at room temperature, and then, the temperature was elevated up to 100 °C. The mixture was heated for 7 h. After the mixture was cooled to room temperature, 30 mL of water and 1 mL of concentrated HCl were added. The precipitate was collected, washed with methanol, and dried in the oven at 60 °C for 2 h. The solid was recrystallized from a dichloromethane/hexane mixture. Yield, 0.7063 g (62%). MS-EI *m/z* 244 [$M^+$, calculated for $C_{13}H_8O_3S$]. $^1$H NMR (DMSO-$d_6$, 300 MHz) $\delta$ ppm: 8.58 (dd, $J_1 = 8.7$ Hz, $J_2 = 7.5$ Hz, 2H), 8.44 (d, $J = 7.8$ Hz, 1H), 7.93 (dd, $J_1 = 7.5$ Hz, $J_2 = 8.7$ Hz, 1H), 7.71 (d, $J = 7.8$ Hz, 1H), 3.33 (s, 3H). $^{13}$C NMR (DMSO-$d_6$, 75 MHz) $\delta$ ppm: 161.2, 161.0, 148.3, 133.2, 132.7, 130.8, 130.1, 128.6, 127.9, 122.2, 120.1, 114.9, 14.6.

**Preparation of MeS-NI (6-methylsulfanylbenzo[de]isoquinoline-1,3-dione).** A suspension of compound **III** (0.2 g) in 7 mL of formamide was placed in a microwave reactor (CEM Discover). Applied were the following parameters: power, 250 W; $T = 200$ °C; $p = 150$ psig, for 10 min. The formed solution was poured into 20 mL of water. The dark brown precipitate was collected, recrystallized from ethanol, and dried in the oven. The crude MeS-NI was purified by column chromatography (silica gel 60, 190 mm × 60 mm column; eluent, a mixture of $CH_2Cl_2$/methanol in a 10/1 ratio). Yield, 0.2264 (80%). MS-EI *m/z* 243 [$M^+$, calculated for $C_{13}H_9O_2NS$]. $^1$H NMR (DMSO-$d_6$, 300 MHz) $\delta$ ppm: 11.70 (s, 1H), 8.49 (dd, $J_1 = 8.1$ Hz, $J_2 = 7.2$ Hz, 2H), 8.34 (d, $J = 7.8$ Hz, 1H), 7.88 (dd, $J_1 = 7.5$ Hz, $J_2 = 8.4$ Hz, 1H), 7.66 (d, $J = 7.8$ Hz, 1H), 2.74 (s, 3H). $^{13}$C NMR (75 MHz DMSO-$d_6$) $\delta$ ppm: 164.4, 146.4, 130.8, 130.3, 129.8, 129.1, 128.9, 127.5, 123.7, 121.9, 118.9, 14.6.

**Preparation of $Me_2N$-NI (6-dimethylaminobenzo[de]isoquinoline-1,3-dione).** A suspension of compound **II** (0.2 g) and 7 mL of formamide was placed in a microwave reactor (CEM Discover). Aplied were the following parameters: power, 250 W; $T = 200$ °C; $p = 150$ psig, for 10 min. The formed solution was poured into 20 mL of water. The dark brown precipitate was collected, recrystallized from ethanol, and dried in the oven. Yield, 0.0882 g (57%). MS-EI *m/z* 240 [$M^+$, calculated for $C_{14}H_{12}O_2N_2$]. $^1$H NMR (300 MHz DMSO-$d_6$) $\delta$ ppm: 8.49 (d, $J = 8.4$ Hz, 1H), 8.40 (d, $J = 7.5$ Hz), 8.29 (d, $J = 8.1$ Hz, 1H), 7.74 (dd, $J_1 = 7.5$ Hz, $J_2 = 8.1$ Hz, 1H), 7.20 (d, $J = 8.1$ Hz, 1H), 3.07 (s, 6H). $^{13}$C NMR (75 MHz DMSO-$d_6$) $\delta$ ppm: 164.8, 164.2, 157.1, 131.9, 131.4, 130.3, 125.4, 125.2, 123.3, 114.5, 113.5, 44.9.

**UV/Vis Steady-State Measurements.** NI solutions for the absorption measurements were prepared at a concentration of ~0.3 mM. Absorption spectra were recorded on Agilent 8453 UV spectrometer in a 2 mm quartz cell. For emission measurements, the concentration of each NI solution was such that the absorption at the wavelength of maximum absorption was in the 0.1−0.15 range. Fluorescence spectra were recorded at Edinburg Instruments Fluorimeter with a Xe900 lamp in 10 mm quartz cells.

**Transient Absorption Measurements.** The laser system for the ultrafast transient absorption measurement was described previously.[18] Briefly, the 800 nm laser pulses were produced at a 1 kHz repetition rate by a mode-locked Ti:Sapphire laser (Hurricane, Spectra-Physics). The pulse width was determined to be fwhm = 110 fs using an autocorrelator (Positive Light). The output from a Hurricane was split into pump (85%) and probe (8%) beams. The pump beam (800 nm) was sent into a second harmonic generator (Super Tripler, CSK) to obtain a 400 nm excitation source. The energy of the pump beam was ~5 $\mu$J/pulse. The probe beam (800 nm) was delayed by a delay stage (MM 4000, Newport) and then focused into a Sapphire crystal for white light continuum generation between 450 and

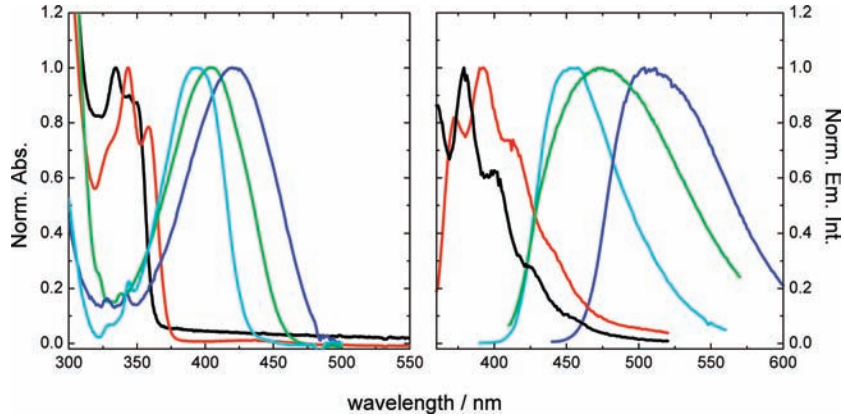


**Figure 1.** Absorption and emission spectra of NI and its derivatives in $CH_2Cl_2$ solutions: NI (black), Cl-NI (red), SMe-NI (cyan), $NO_2$-NI (green), and $NMe_2$-NI (blue).

900 nm. An optical chopper was used to modulate the excitation beam at 100 Hz frequency and obtain the value of the transient absorption signal. The relative polarization between the pump and probe beams was set at the magic angle (54.7°). The pump and probe beams were overlapped in the sample. The flow cell (Spectrocell Inc., 0.7 mL volume with 2 mm path length), pumped by a Fluid Metering RHSY Lab pump (Scientific Support Inc.), was used to minimize the effects of photodegradation of the sample on the observed spectra. After passing through the flow cell, the continuum was coupled into an optical fiber and input into a CCD spectrograph (Ocean Optics, S2000). The data acquisition was achieved using in-house LabVIEW (National Instruments) software routines.

**Data Processing and Analysis.** The transient absorption data were processed as follows: (i) The chirp correction was done using optical Kerr effect, (ii) the noise was reduced using a singular value decomposition (SVD) method, and (iii) data were analyzed using kinetic models by global analysis. The details of all of these procedures were published previously.[19,20]

**Computational Methods.** All of the calculations were performed with the Turbomole-5.80 suite of programs,[21,22] unless otherwise noted. The ground-state geometries were optimized using Becke's three-parameter hybrid exchange functional with the Lee−Yang−Parr correlation functional (B3LYP) method[23] in conjunction with the 6-31+G* basis set.[24] The optimized ground-state geometries were confirmed to be minima on their respective potential energy surfaces by calculating the analytical second derivatives of the energy using the AOFORCE module,[25] as implemented in the Turbomole suite. Computations of the vertical excitations, difference density plots, and optimization of the excited states were performed using time-dependent DFT,[26] using the B3LYP functional (TD-B3LYP) and the 6-31+G* basis set. The optimized geometries on the excited-state potential energy surfaces were characterized by calculating the second derivatives of the energy by numerical differentiation of the analytical first derivative with the NUMFORCE module in Turbomole. Such vibrational frequency analyses were used to characterize the stationary points on the excited-state surfaces and confirmed each stationary point to be a minimum on the respective surface. The effects of solvation on the vertical excitation energies were computed with Tomasi's polarizable continuum model (PCM)[27−32] at the TD-B3LYP/ 6-31+G* level of theory as implemented in Gaussian 03.[33]

## Results and Discussion

**Synthesis.** Scheme 2 presents the procedure for preparation of $M_2N$-NI and MeS-NI. The method is based on the nucleophilic aromatic substitution of a chloro-substituted naphthalene derivative with $Me_2N$ or MeS groups. It was not possible to use chloronaphthalimide as a starting material since the N-H group of NIs could react with the base used in the aromatic substitution. Instead, the starting material for reaction was the anhydride derivative **I**. After the Cl group was substituted by $Me_2N$ or MeS groups, the corresponding anhydrides were converted into imides using formamide in a procedure similar to the one reported for a variety of cyclic anhydrides.[34]

**UV/Vis Absorption and Fluorescence Measurements.** Figure 1 presents the absorption and fluorescence spectra of five NI derivatives. The absorption maximum for NI appears at 350 nm, while its fluorescence emerges at 400 nm. Chloro substitution in the 4-position leads to minor changes in the absorption and emission spectra. A small red shift is observed in the spectra of Cl-NI relative to NI. The nature of the chloro substituent is unusual: It is an electron-donating substituent due to its lone pair of electrons, while it behaves as an electron-withdrawing substituent due to the relative electronegativity of Cl atom. Thus, the overall effect of Cl substitution is minor, and the character of the excited state is very similar to the parent NI. Substitution by −SMe, $-NO_2$, and $-NMe_2$ groups leads to a more drastic change in the absorption and emission spectra: (i) A large red shift is observed relative to the spectra of NI, and (ii) the absorption and emission bands become broad and structureless. These results are consistent with the presence of the CT excited states. In the case of $Me_2N$-NI and MeS-NI, the charge transfer occurs from the 4-substituent toward the aromatic ring. The charge transfer in $O_2N$-NI occurs in the opposite direction: from aromatic ring toward the nitro substituent.

To further investigate the nature of the excited states in five NI derivatives, we studied the effect of solvent polarity on the absorption and emission maxima. The correlation between the solvent polarity and the absorption and emission maximum shift is described by Lippert equations:[35]

$$h\nu_{\mathrm{Abs}} = h\nu_{\mathrm{o}}^{\mathrm{Abs}} - \frac{2\mu_{\mathrm{g}}(\mu_{\mathrm{e}} - \mu_{\mathrm{g}})}{a_{\mathrm{o}}^3} \times f(\varepsilon, n) \qquad (1)$$

$$h\nu_{\mathrm{Em}} = h\nu_{\mathrm{o}}^{\mathrm{Em}} - \frac{2\mu_{\mathrm{e}}(\mu_{\mathrm{e}} - \mu_{\mathrm{g}})}{a_{\mathrm{o}}^3} \times f(\varepsilon, n) \qquad (2)$$

Here, $h\nu_{\mathrm{Abs}}$ and $h\nu_{\mathrm{Em}}$ are the absorption and emission energies of the molecule in a given solvent; $h\nu_{\mathrm{o}}^{\mathrm{Abs}}$ and $h\nu_{\mathrm{o}}^{\mathrm{Em}}$ are the corresponding energies in the vacuum; $\mu_{\mathrm{g}}$ and $\mu_{\mathrm{e}}$ are dipole

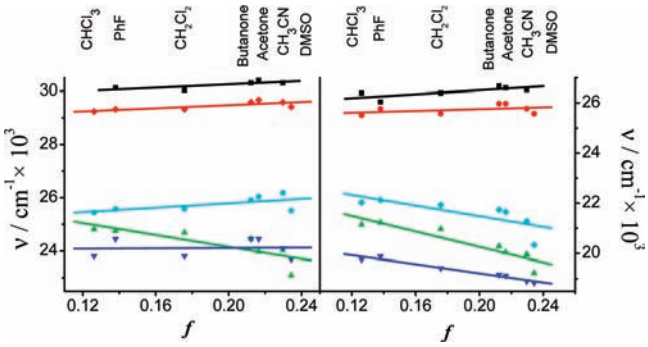


**Figure 2.** Plot of the absorption (left) and emission (right) maxima of five NIs as a function of solvent's *f* function (eqs 1 and 2): NI (black), Cl-NI (red), SMe-NI (cyan), $NO_2$-NI (green), and $NMe_2$-NI (blue).

moments for a molecule in the ground and excited states, respectively; $a_o$ is the molecular Onsager radius; $f(\varepsilon,n)$ is a function that depends on the dielectric constant ($\varepsilon$) and refractive index ($n$) of the solvent and is expressed as:

$$f(\varepsilon, n) = \frac{\varepsilon - 1}{2\varepsilon + 1} - \frac{1}{2}\frac{n^2 - 1}{2n^2 + 1} \qquad (3)$$

The Lippert equation shows that a chromophore's sensitivity to solvent polarity arises due to the changes in the molecule's excited-state dipole moment relative to its dipole moment in the ground state. If no net change in dipole moment occurs ($\mu_e - \mu_g = 0$), the absorption and emission maxima of the chromophore should not change with increased solvent polarity. If the excited-state dipole moment is larger than that of ground state ($\mu_e - \mu_g > 0$), the absorption and emission maxima should red shift with the increased solvent polarity. This situation occurs in compounds that exhibit CT and $\pi,\pi^*$ excited states. On the other hand, if the dipole moment decreases upon excitation ($\mu_e - \mu_g < 0$), the absorption and emission maxima are expected to show a blue shift with increased polarity of solvent. This blue shift occurs in molecules with n,$\pi^*$ excited states.

Figure 2 plots the changes in the absorption and emission maxima of five NIs as a function of the solvent's *f* function. The absorption maxima show a slight blue shift (positive slope) with increased solvent polarity for all NIs except in the case of $O_2$N-NI. This behavior is consistent with the n,$\pi^*$ excited state. In the computational section, we will show that the calculated $S_1$ state in NIs exhibits a $\pi,\pi^*$ character, while the $S_2$ excited state has an n,$\pi^*$ character. If the light absorption produced the $S_1$ ($\pi,\pi^*$) excited state, DFT calculations predict a negative Lippert slope for all NIs (Table 3). On the other hand, the excitation to $S_2$ state (n,$\pi^*$) is expected to give rise to a positive slope for all NIs except $O_2$N-NI, where a negative slope is calculated. It is interesting that the experimental results presented in Figure 2 correlate well with the slopes predicted for the excitation to $S_2$ state with n,$\pi^*$ character except for $O_2$N-NI. Thus, we conclude that the absorption of light produces dominantly the $S_2$ excited state in these NIs.

The effect of solvent polarity on the emission maxima is not equivalent to the one observed with the absorption maxima. For example, MeS-NI exhibits a blue shift of the absorption maximum with increased solvent polarity, whereas a red shift is observed for its emission maximum (Figure 2). This result clearly demonstrates that the emissive state in MeS-NI is not the same as the one produced upon light absorption. As we described previously, the absorption of light produces the $S_2$ (n,$\pi^*$) state. From the emission data, we conclude that fast $S_2$ to $S_1$ internal conversion occurs in $O_2$N-NI, MeS-NI, and $Me_2$N-NI. The fluorescence then arises from the $S_1$ ($\pi,\pi^*$) state, which is expected to show a red shift with increased solvent polarity. It is interesting to note that NI and Cl-NI do not exhibit this behavior. Both the absorption and the emission maxima for NI and Cl-NI show a blue shift with increased solvent polarity, which is consistent with the n,$\pi^*$ excited state and a rapid internal conversion rate from this state.

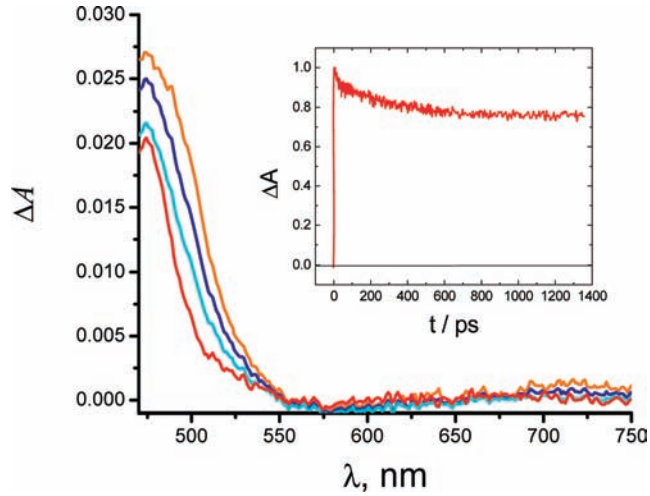


**Figure 3.** Transient absorption spectrum of N in dichloromethane obtained at different probe delays: 5 (orange), 100 (blue), 400 (cyan), and 1200 ps (red). Inset: NI excited-state decay obtained at $\lambda = 475$ nm.

**Transient Absorption.** Figure 3 presents the transient absorption spectrum of NI in dichloromethane. At initial time, the spectrum consists of an absorption band centered at ~475 nm that is assigned to the $^1$(n,$\pi^*$) state. This is not consistent with the previously published work,[16] where the authors assign this state to $^1$($\pi,\pi^*$). However, on the basis of the above-described solvent dependence on the absorption and emission maxima of NI, we believe it is more appropriate to assign the transient absorption signal to the $^1$(n,$\pi^*$) state. The $^1$(n,$\pi^*$) absorption decays with a lifetime of 0.4 ns and a new long-lived absorption band appears in the same spectral region. The features of this long-lived species can be observed in the spectrum collected at a time delay of $t = 1200$ ps. Here, we can see that the absorption is blue-shifted relative to the absorption of the initial $^1$(n, $\pi^*$) state. We assign this absorption band to the triplet excited state of NI. Similarly to ground-state absorption and emission spectra of NI derivatives, the Cl substitution in the 4-position leads to a very small change in the transient absorption spectrum (data not shown). The absorption maximum of the $^1$(n,$\pi^*$) state of Cl-NI is slightly red-shifted relative to NI. However, the $^1$(n,$\pi^*$) excited-state lifetime is the same for both NI and Cl-NI ($\tau = 0.4$ ns). To obtain the absorption spectra of $^1$(n,$\pi^*$) and $^3$($\pi,\pi^*$) states, we decomposed the transient absorption data using a $^1S \rightarrow {}^3T$ kinetic model (global analysis). The deconvoluted spectra for NI and Cl-NI are presented in Figure 4. In both cases, the $^1$(n,$\pi^*$) state absorbs at a somewhat higher wavelength than the $^3$($\pi,\pi^*$) state.

Contrary to Cl-NI, the excited-state behavior of $Me_2$N-NI, $O_2$N-NI, and MeS-NI are drastically different from that of NI. Figure 5 presents the transient absorption data in solutions of varying polarity. Qualitatively, all three NIs exhibit similar features: a stimulated emission peak that appears in the 500−550 nm range and an excited-state absorption in the red portion of the spectrum (600−750 nm). As expected, the increased solvent

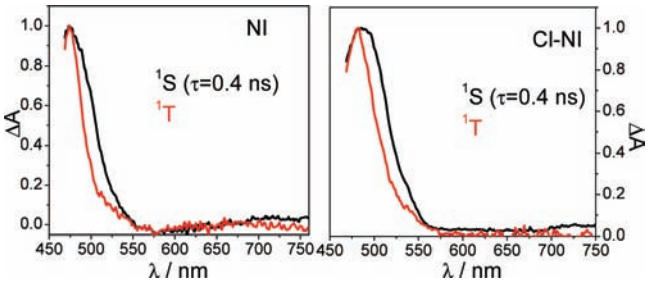


**Figure 4.** Absorption spectra of singlet and triplet excited states in N (left) and Cl-NI (right). The spectra were obtained from transient absorption data using Specfit software (Experimental Section).

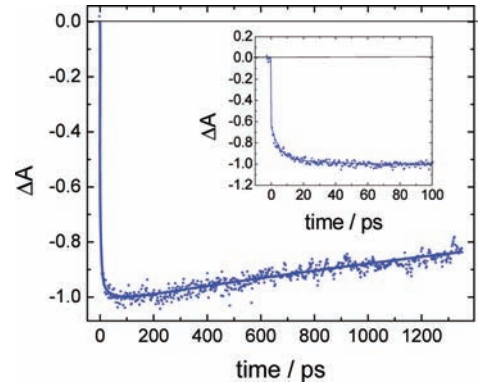


**Figure 6.** Decay of stimulated emission signal at 525 nm for $N_2$-NI in chloroform (scatter). The solid line represents the fit obtained using a double-exponential function with the risetime of $\tau = 40$ ps and a decay time of $\tau = 3.9$ ns convolved with an instrument response function.

polarity gives rise to a red shift of the stimulated emission band in $O_2$N-NI and $Me_2$N-NI. In the case of MeS-NI, the stimulated emission peak appears to blue shift. This behavior is due to the contribution from the excited-state absorption in the stimulated emission range. With increased solvent polarity, the energy of the singlet excited state decreases, which leads to a red shift of the stimulated emission peak and a blue shift of the excited-state absorption peak. The overall effect of these two shifts gives rise to the observed blue shift of the stimulated emission signal. In accordance with the computational results presented in the next section, we assign the excited state in $Me_2$N-NI, $O_2$N-NI, and MeS-NI to a CT state.

In chloroform, the solvent with the lowest dielectric constant in these studies, all three NIs exhibit the same excited-state dynamics. As an example, we present the stimulated emission dynamics for $O_2$N-NI in Figure 6. The signal exhibits a rise with the lifetime of 40 ps and a long decay with the lifetime of 3.9 ns. One possible explanation for the short-lived rise component is solvation dynamics. Because the excited state has a CT character, a large redistribution of charges upon excitation is expected to be followed by significant redistribution of the solvent dipoles. However, the solvation dynamics usually lead to a red shift in the stimulated emission peaks, which is not the case for our data. We believe that the short-lived component arises due to internal conversion from the $^1(n,\pi^*)$ to the CT excited state of NI derivatives (Scheme 3). This assignment is

**SCHEME 3: $S_2-S_1$ Internal Conversion in SMe-NI[a]**

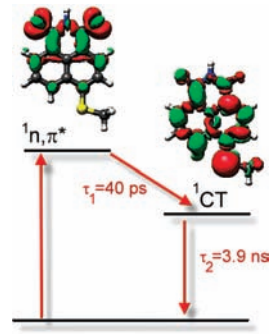


[a] The difference energy plots for two excited states were obtained using the TD-DFT method (red color, electronic density depleted in the excited state; green color, electronic density increased in the excited state).

supported by the above-described absorption and emission experiments in solvents of varying polarity, which suggest that NI derivatives create the $^1(n,\pi^*)$ excited state ($S_2$) upon absorption, while the emission in $Me_2$N-NI, $O_2$N-NI, and MeS-

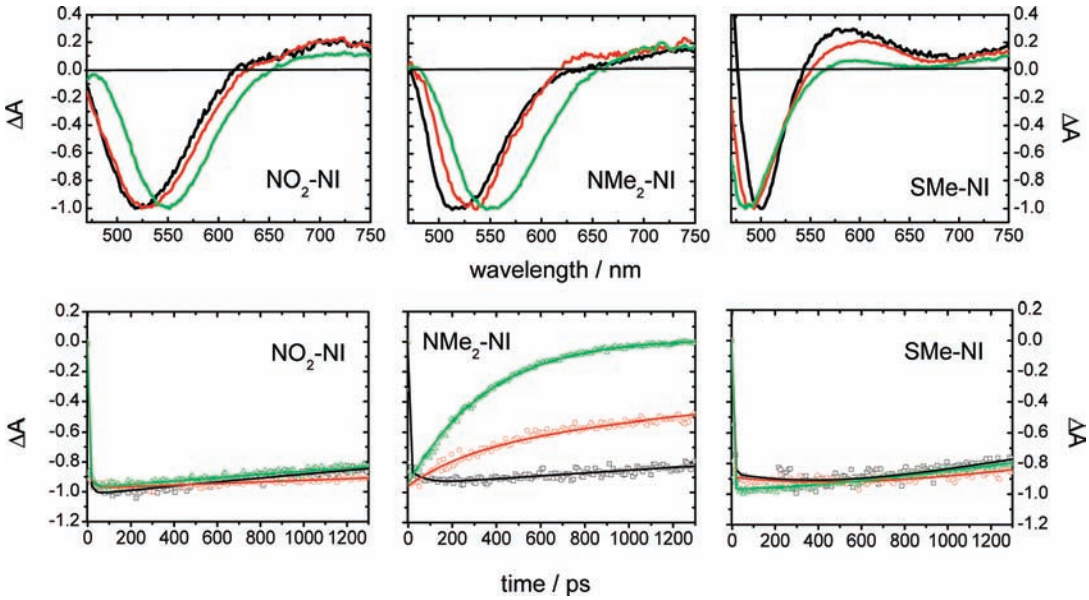


**Figure 5.** Transient absorption spectra for $N_2$-NI, $NMe_2$-NI, and SMe-NI collected 50 ps after the excitation pulse (upper panels) and the decay of stimulated emission signal of $NO_2$-NI, $NMe_2$-NI, and SMe-NI (lower panels). The solvents used were as follows: chloroform (black lines), dichloromethane (red lines), and acetonitrile (green lines).

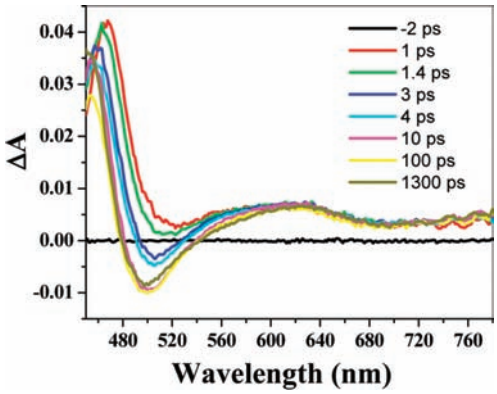


**Figure 7.** Transient absorption spectra of SMe-N in chloroform. The spectra were collected at different delay times after the 420 nm excitation pulse.

NI occurs from the CT excited state ($S_1$). From these data, it is obvious that the conversion between these two states must occur upon excitation. Thus, we assign the 40 ps component to the $S_2 \rightarrow S_1$ internal conversion. The confirmation for this assignment can be best observed from transient absorption spectra of MeS-NI obtained upon excitation by a 420 nm (Figure 7). The spectrum obtained 1 ps after the excitation pulse consists of two positive signals centered at 470 and 620 nm and arises due to the absorption of the $S_2$ excited state of MeS-NI. The spectra obtained at subsequent time delays clearly show a growth of the stimulated emission signal centered at 500 nm, which is a signature of the $S_1$ CT excited state. The n,$\pi^*$ transitions are generally considered quasi-forbidden: They are allowed by symmetry but exhibit a small overlap between n and $\pi^*$ orbitals. For these reasons, the deactivation of n,$\pi^*$ states usually involves a thermal deactivation via conical intersection with the lower-lying states. In the case of MeS-NI, we were unable to calculate the $S_2-S_1$ conical intersection using a DFT method, so we cannot discuss the exact vibrational motion that leads to the $S_2-S_1$ conversion. However, it is known that n, $\pi^*$ excited states of simple aldehydes are pyramidalized about the C−O bond in the excited state.[36] Thus, we postulate that the out-of-plane bending motions of C−O bond or in-plane distortions due to the change in bond lengths lead to a deactivation mechanism for the excited states.

An interesting effect is observed in the excited state dynamics of $Me_2N$-NI as a function of solvent polarity. While MeS-NI and $O_2N$-NI excited-state dynamics do not change when the solvent is changed from chloroform to dichloromethane and acetonitrile, the decay of $Me_2N$-NI becomes faster (Figure 5, lower panels). The lifetime decreases from 3.9 ns in chloroform to only 360 ps in acetonitrile. We assign this lifetime shortening to the excited-state rotation of the $Me_2N$ group relative to the aromatic ring. As will be discussed in the following section, the 4-substituent in $Me_2N$-NI is at a small angle relative to the aromatic ring in the ground-state optimized geometry. The situation is different in the optimized excited-state geometry, where the 4-substituent is at a 90° angle (twisted state). Thus, a rotation of the 4-substituent is expected to occur along the $^1S$ potential energy surface. In nonpolar environment, the highly polar twisted excited state is not stabilized by the solvent, leading to transient absorption by the initially produced $\pi,\pi^*$ excited state. As the solvent polarity is increased, the twisted state becomes stabilized, leading to a fast deactivation of the initially produced $\pi,\pi^*$ excited state (Scheme 4). A similar effect has been observed previously with $Me_2N$ derivatives of various aromatic compounds.[37,38] In these reports, the authors observed

**SCHEME 4: Schematic Representation of the Effect of Solvent Polarity on the Energy of $S_1$ State in $NMe_2$-NI**

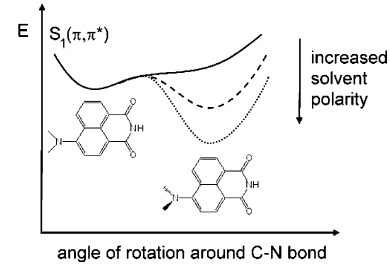


**TABLE 1: Comparison of Experimental Absorption Maxima of Five NIs with Those Calculated Using TD-DFT for $S_1$ and $S_2$ Excited States[a]**

| | $\lambda_{exp}$ (nm) | $\lambda_{calcd}$ (nm) | |
|---|---|---|---|
| | | S1 | S2 |
| NI | 337 | 345 | 337 |
| Cl-NI | 356 | 348 | 348 |
| SMe-NI | 391 | 390 | 345 |
| $NO_2$-NI | 405 | 379 | 369 |
| $NMe_2$-NI | 416 | 404 | 342 |

[a] The experimental values in vacuum were obtained as *y*-intercepts of Lippert plots (Figure 2 and eq 1).

dual fluorescence arising from "twisted" and "planar" excited states. The dual emission occurred only in solvents with high solvent polarity, which is consistent with our data. We did not observe any signal from the twisted state in neither fluorescence nor transient absorption spectra.

**Time-Dependent (TD)-DFT Calculations.** The calculations of the ground- and excited-state properties of NI derivatives were performed using TD-DFT[26] as implemented in Turbomole software,[21,22] along with the B3LYP[23,39,40] functional and the 6-31+G* basis set.[24] To validate the computational method, we first compared the calculated electronic absorption maxima of NI derivatives with those obtained experimentally (Table 1). While the computations were performed without corrections for solvent effects, the experiments were done in various solvents. To compensate for the disagreement in absorption maxima due to solvent effects, the "experimental" vacuum absorption maxima were obtained as *y*-intercepts in Lippert plots (Figure 2 and eq 1). Table 1 compares these experimental values with the calculated absorption maxima for the $S_1$ and $S_2$ excited states of five NI derivatives. The experimental values agree very well with the calculated $S_1$ excitation energies for all NIs except in the case of the parent NI where the absorption maximum correlates better with the calculated $S_2$ energy. As we will see in the following discussion, all of the experimental values correlate well with the calculated $\pi,\pi^*$ excitation energies.

Figure 8 presents the difference density plots for $S_1$ and $S_2$ excited states of five NI derivatives. We have recently utilized difference density plots to elucidate several different photochemical processes,[41−44] which is a strategy to visualize the changes in electron density upon vertical excitation, especially for states that are described by contributions from multiple occupied to unoccupied orbital configurations. In the case of NI, the $S_1$ excited state is characterized by electronic charge depletion from the lone electron pairs of the imide oxygen atoms and a charge accumulation on the aromatic rings. This sort of difference density plot is characteristic of an n,$\pi^*$ excited state, which is additionally supported by the small oscillator strength for this transition ($f = 0.0001$). The change in electron density for the $S_2$ excited state in NI alternates in sign on the conjugated

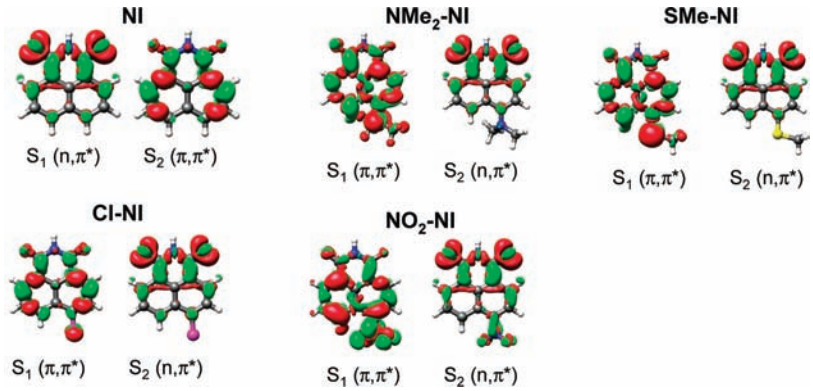


**Figure 8.** Calculated difference density plots for $S^1$ and $S_2$ states of five NI derivatives. The red surfaces correspond to depletion of electron density from $S_0$ state. The green surfaces correspond to the areas of accumulation of electron density.

**SCHEME 5: Calculated Energies of n,$\pi^*$ and $\pi,\pi^*$ States of N in Vacuum and Dichloromethane**

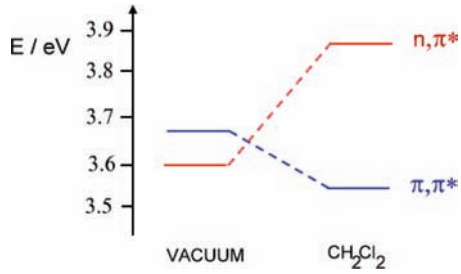


system, which is characteristic of the $\pi,\pi^*$ excited state. In the case of other NI derivatives, the order of excited states is switched, with the $S_1$ state having a $\pi,\pi^*$ character and $S_2$ state having an n,$\pi^*$ character.

Returning to the results presented in Table 1, we can see that all of the experimental absorption maxima correlate well with the calculated absorption energies to produce $\pi,\pi^*$ states. The unusual result is observed in the case of NI, where the experimental absorption wavelength correlates better with the calculated $S_2$ energy. To understand the reason for this behavior, we conducted a DFT calculation for NI using the PCM model[27−32] for dichloromethane as implicit solvent. We found that the solvent stabilizes the $\pi,\pi^*$ excited state and destabilizes the n,$\pi^*$ state, which leads to a reversal of order of these two energy levels (Scheme 5). Given this reversal of states, it is understandable why our experimental absorption maxima correlate better with the calculated $S_2$ energy in vacuum. Even though our experimental absorption maxima were extrapolated from Lippert plots to the vacuum values, this extrapolation is based on the assumption that the reversal of states does not occur. Thus, all NI derivatives exhibit $\pi,\pi^*$ excited state as the lowest singlet excited state.

We further calculated the optimized geometries on the excited-state potential energy surfaces, which were confirmed to be minima by calculating the second derivatives of the energy by numerical differentiation of the analytical first derivative with the NUMFORCE module in Turbomole.[21,22] Comparisons of calculated emission energies with the experimental fluorescence maxima are presented in Table 2. As with the absorption values, the experimental emission maxima were obtained as *y*-intercepts in Lippert plots (Figure 2). Because of the reversal of states described previously, the value used for NI is the calculated energy of the $S_2$ excited state. For the rest of NI derivatives, we used energies of the optimized $S_1$ states. The agreement between experiment and theory is satisfactory for NI, Cl-NI, and MeS-NI, while the calculated energies for optimized $Me_2N$-NI and $O_2N$-NI excited states are significantly lower than the experimentally observed. An interesting finding is that NI derivatives in which the experimental and calculated emission energies do not correlate well are those that are expected to undergo a large change in geometry during the excited state's relaxation. The difference between the calculated Franck−Condon and relaxed geometries of $S_1$ states in NI, Cl-NI, and MeS-NI is only in their bond lengths. On the other hand, the relaxation of the $S_1$ states of $O_2N$-NI and $Me_2N$-NI involves a rotation of the 4-substituent around the C−N bond (Figure 9). The ground-state geometry of $O_2N$-NI involves the $NO_2$ group at 38° out of the aromatic plane. Upon excitation, a charge transfer from aromatic rings to the $NO_2$ group drives the formation of a planar quinoidlike structure. The opposite effect occurs in the case of

**TABLE 2: Comparison of Experimental Fluorescence Maxima of Five NIs with Those Calculated Using TD-DFT for the $S_1$ Excited State[a]**

| | $\lambda_{exp}$ (nm) | $\lambda_{calcd}$ (nm) |
|---|---|---|
| NI | 389 | 420[b] |
| Cl-NI | 372 | 386 |
| SMe-NI | 452 | 430 |
| $NO_2$-NI | 477 | 830 |
| $NMe_2$-NI | 475 | 644 |

[a] The experimental values in vacuum were obtained as *y*-intercepts of Lippert plots (Figure 2). [b] The value obtained for the $S_2$ excited state.

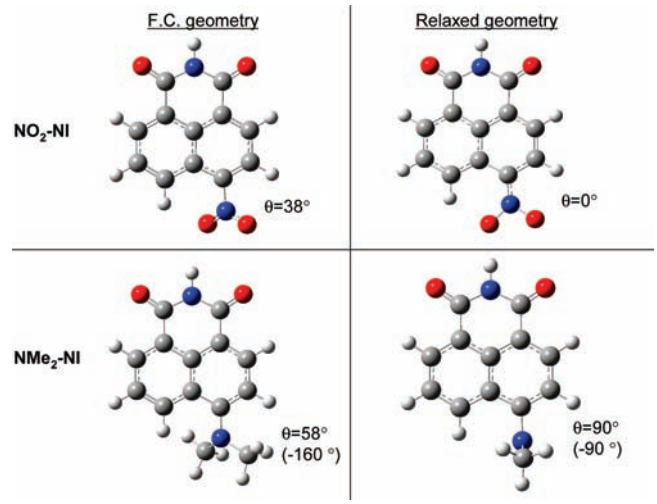


**Figure 9.** Calculated geometries for Franck−Condon and relaxed $S_1$ states of $NO_2$-NI and $NMe_2$-NI. The angle $\theta$ is a dihedral angle between the plane of the aromatic rings and the N-O/N-Me bonds of 4-substituents in $NO_2$-NI and $NMe_2$-NI, respectively.

**TABLE 3: Calculated Lippert Slopes for Absorption to $S_1$ and $S_2$ States of NI Derivatives**

| | | | $\mu_e$ (D) | | $-[2\mu_g(\mu_e - \mu_g)/a_o^3]$ (eV) | |
|---|---|---|---|---|---|---|
| | $r$ (Å) | $\mu_g$ ($S_0$) (D) | $\pi,\pi^*$ | n,$\pi^*$ | $\pi,\pi^*$ | n,$\pi^*$ |
| NI | 4.59 | 5.41 | 6.4 | 0.36 | −0.03 | 0.17 |
| Cl-NI | 4.81 | 3.84 | 5.42 | 1.5 | −0.03 | 0.05 |
| SMe-NI | 5.07 | 6.35 | 11.3 | 1.6 | −0.15 | 0.14 |
| $NO_2$-NI | 4.76 | 1.17 | 4.36 | 6.9 | −0.02 | −0.04 |
| $NMe_2$-NI | 5.02 | 7.89 | 11.9 | 2.5 | −0.15 | 0.20 |

$Me_2N$-NI, where the charge transfer is primarily localized from the $NMe_2$ group to the aromatic ring and the CT state is stabilized by a twisted geometry.

The emission from relaxed $S_1$ states of $O_2N$-NI and $Me_2N$-NI is expected to occur at lower energies than observed. The calculated emission wavelengths of $O_2N$-NI and $Me_2N$-NI are 830 and 644 nm, while the observed fluorescence maxima occur at 477 and 475 nm, respectively. We believe that the disagreement between these values arises due to the fact that excited $O_2N$-NI and $Me_2N$-NI emit light before achieving their relaxed excited state geometry, suggesting a high activation barrier for rotation around C−N bonds.

Another possibility for the disagreement between experiment and theory can be found in the failure of the TD-DFT method in describing CT states.[45] The TD-DFT method has become popular among chemists due to its low computational demand. However, the TD-DFT method applies approximate ground-state exchange-correlation functions, which give potentials with incorrect dependence on the electron−nucleus distance. The outcome of applying the TD-DFT method to CT states is that the calculated excitation energies are thus underestimated. This is exactly the case for our system. The calculated emission energies (for example, 830 nm for $O_2N$-NI) are much lower than the experimentally observed (477 nm for $O_2N$-NI).

On the basis of the analysis of the absorption and emission maxima, we can conclude that the excited-state properties of NI derivatives can be well-described by a $\pi,\pi^*$ excited state. However, the experiments on the effect of solvent polarity on absorption and emission maxima as well as the transient absorption data suggest that the excitation of NIs creates n,$\pi^*$ $S_2$ states, which decay to $\pi,\pi^*$ excited states within several picoseconds. To demonstrate this behavior, Table 3 presents the calculated slopes of the Lippert plots for absorption to $S_1$ and $S_2$ states of NIs. We can see from Table 3 that the excitation to $\pi,\pi^*$ state should give rise to negative slopes for all five Nis, while the excitation to n,$\pi^*$ should give rise to positive slopes for all NIs except in the case of $NO_2$-NI, where a negative slope is expected (highlighted column in the Table 3). Our experimental slopes (Figure 2) correlate with the calculated slopes for the n,$\pi^*$ transition.

## Conclusions

This paper describes a study of excited-state properties of a series of NI and 4-substituted NI derivatives. The type of the substituent was varied from electron-withdrawing groups, such as $NO_2$ to electron-donating groups, such as $NMe_2$. We obtained a series of steady-state absorption and fluorescence spectra of the NI derivatives in solvents of varying polarity. We found that the absorption of light created the $S_2$ excited state. The character of this state was determined to have a n,$\pi^*$ character by means of TD-DFT calculations. Using ultrafast transient absorption experiments, we found that the initially produced $S_2$ excited state undergoes internal conversion within 40 ps to produce the $S_1$ excited state. This state has a $\pi,\pi^*$ character in NI and Cl-NI, while it has a CT character in $O_2N$-NI, $Me_2N$-NI, and MeS-NI. In compounds with CT states, the excited state lifetimes are relatively long (3.9 ns).

We compared the experimental absorption and emission maxima for all NI derivatives with those calculated using the TD-DFT method. We find excellent agreement in all of the values, except for the fluorescence maxima of $Me_2N$-NI and $O_2N$-NI. In both of these compounds, the experimental fluorescence maxima have higher energy than the calculated maxima. An interesting finding is that this discrepancy between experiment and theory arises with the compounds that are expected to have a large structural change in the excited state. In the case of $Me_2N$-NI, the rotation of the $NMe_2$ group is expected to occur to produce a twisted excited state, while in $O_2N$-NI, the rotation of the $NO_2$ group is expected to produce a planar excited state. Thus, we believe that the discrepancy arises due to the fluorescence from the nonequilibrated excited state. A detailed computational study describing the geometrical changes in the excited state and infrared frequencies of the excited states along with the adiabatic and relaxed energetics for all five NIs will be presented in due course.

**Acknowledgment.** We gratefully acknowledge the Ohio Laboratory for Kinetic Spectrometry, where the pump−probe laser measurements were conducted. We also gratefully acknowledge generous computational resources from the Ohio Supercomputer Center. K.D.G. thanks ACS Petroleum Research Fund for the financial support (46807-G4). C.M.H. thanks the National Science Foundation for financial support.

## References and Notes

(1) Rogers, J. E.; Kelly, L. A. *J. Am. Chem. Soc.* **1999**, *121*, 3854–3861.
(2) Saito, I.; Takayama, M.; Kawanishi, S. *J. Am. Chem. Soc.* **1995**, *117*, 5590–5591.
(3) Alexiou, M. S.; Tychopoulos, V.; Ghorbanian, S.; Tyman, J. H. P.; Brown, R. G.; Brittain, P. I. *J. Chem. Soc.-Perkin Trans. 2* **1990**, 837–842.
(4) Aveline, B. M.; Matsugo, S.; Redmond, R. W. *J. Am. Chem. Soc.* **1997**, *119*, 11785–11795.
(5) Chanh, T. C.; Lewis, D. E.; Allan, J. S.; Sogandaresbernal, F.; Judy, M. M.; Utecht, R. E.; Matthews, J. L. *Aids Res. Hum. Retroviruses* **1993**, *9*, 891–896.
(6) Zhang, J. X.; Woods, R. J.; Brown, P. B.; Lee, K. D.; Kane, R. R. *Bioorg. Med. Chem. Lett.* **2002**, *12*, 853–856.
(7) Skurla, C. P.; Perera, A.; Towe, C. T.; Robertson, P. R.; Healy, J. L.; Kane, R. R. *J. Biomech.* **2007**, *40*, 220–224.
(8) Hasharoni, K.; Levanon, H.; Greenfield, S. R.; Gosztola, D. J.; Svec, W. A.; Wasielewski, M. R. *J. Am. Chem. Soc.* **1996**, *118*, 10228–10235.
(9) Kolosov, D.; Adamovich, V.; Djurovich, P.; Thompson, M. E.; Adachi, C. *J. Am. Chem. Soc.* **2002**, *124*, 9945–9954.
(10) Ramachandram, B.; Saroja, G.; Sankaran, B.; Samanta, A. *J. Phys. Chem. B* **2000**, *104*, 11824–11832.
(11) He, H. R.; Mortellaro, M. A.; Leiner, M. J. P.; Fraatz, R. J.; Tusa, J. K. *J. Am. Chem. Soc.* **2003**, *125*, 1468–1469.
(12) Guo, X. F.; Qian, X. H.; Jia, L. H. *J. Am. Chem. Soc.* **2004**, *126*, 2272–2273.
(13) Wintgens, V.; Valat, P.; Kossanyi, J.; Demeter, A.; Biczok, L.; Berges, T. *New J. Chem.* **1996**, *20*, 1149–1158.
(14) Wintgens, V.; Valat, P.; Kossanyi, J.; Biczok, L.; Demeter, A.; Berces, T. *J. Chem. Soc.-Faraday Trans.* **1994**, *90*, 411–421.
(15) Pardo, A.; Martin, E.; Poyato, J. M. L.; Camacho, J. J.; Brana, M. F.; Castellano, J. M. *J. Photochem. Photobiol., A* **1987**, *41*, 69–78.
(16) Samanta, A.; Saroja, G. *J. Photochem. Photobiol., A* **1994**, *84*, 19–26.
(17) Zhang, W.; Wang, Y. L.; Xu, Y. F.; Qian, X. H. *Mon. Fur Chem.* **2003**, *134*, 393–402.
(18) Nikolaitchik, A. V.; Korth, O.; Rodgers, M. A. *J. Phys. Chem. A* **1999**, *103*, 7587–7596.
(19) Li, G.; Sichula, V.; Glusac, K. D. *J. Phys. Chem. B* **2008**, *112*, 10758–10764.
(20) Li, G.; Glusac, K. D. *J. Phys. Chem. A* **2008**, *112*, 4573–4583.
(21) Treutler, O.; Ahlrichs, R. *J. Chem. Phys.* **1995**, *102*, 346–354.

(22) Ahlrichs, R.; Bar, M.; Haser, M.; Horn, H.; Kolmel, C. *Chem. Phys. Lett.* **1989**, *162*, 165–169.
(23) Becke, A. D. *J. Chem. Phys.* **1993**, *98*, 5648–5652.
(24) Francl, M. M.; Pietro, W. J.; Hehre, W. J.; Binkley, J. S.; Gordon, M. S.; Defrees, D. J.; Pople, J. A. *J. Chem. Phys.* **1982**, *77*, 3654–3665.
(25) Deglmann, P.; Furche, F.; Ahlrichs, R. *Chem. Phys. Lett.* **2002**, *362*, 511–518.
(26) Olivucci, M. *Computational Photochemistry*; Elsevier: Amsterdam, 2005; pp 92−128.
(27) Tomasi, J.; Persico, M. *Chem. Rev.* **1994**, *94*, 2027–2094.
(28) Cossi, M.; Barone, V. *J. Chem. Phys.* **1998**, *109*, 6246–6254.
(29) Cossi, M.; Barone, V.; Cammi, R.; Tomasi, J. *Chem. Phys. Lett.* **1996**, *255*, 327–335.
(30) Barone, V.; Cossi, M.; Tomasi, J. *J. Chem. Phys.* **1997**, *107*, 3210–3221.
(31) Barone, V.; Cossi, M.; Tomasi, J. *J. Comput. Chem.* **1998**, *19*, 404–417.
(32) Cramer, C. J.; Truhlar, D. G. *Chem. Rev.* **1999**, *99*, 2161–2200.
(33) Frisch, M. J.; Trucks, G. W.; Schlegel, H. B.; Scuseria, G. E.; Robb, M. A.; Cheeseman, J. R.; Montgomery, J. J. A.; Vreven, T.; Kudin, K. N.; Burant; J. C.; Millam, J. M.; Iyengar, S. S.; Tomasi, J.; Barone, V.; Mennucci, B.; Cossi, M.; Scalmani, G.; Rega, N.; Petersson, G. A.; Nakatsuji, H.; Hada, M.; Ehara, M.; Toyota, K.; Fukuda, R.; Hasegawa, J.; Ishida, M.; Nakajima, T.; Honda, Y.; Kitao, O.; Nakai, H.; Klene, M.; Li, X.; Knox, J. E.; Hratchian, H. P.; Cross, J. B.; Bakken, V.; Adamo, C.; Jaramillo, J.; Gomperts, R.; Stratmann, R. E.; Yazyev, O.; Austin, A. J.; Cammi, R.; Pomelli, C.; Ochterski, J. W.; Ayala, P. Y.; Morokuma, K.; Voth, G. A.; Salvador, P.; Dannenberg, J. J.; Zakrzewski, V. G.; Dapprich, S.; Daniels, A. D.; Strain, M. C.; Farkas, O.; Malick, D. K.; Rabuck, A. D.; Raghavachari, K.; Foresman, J. B.; Ortiz, J. V.; Cui, Q.; Baboul, A. G.; Clifford, S.; Cioslowski, J.; Stefanov, B. B.; Liu, G.; Liashenko, A.; Piskorz, P.; Komaromi, I.; Martin, R. L.; Fox, D. J.; Keith, T.; Al-Laham, M. A.; Peng, C. Y.; Nanayakkara, A.; Challacombe, M.; Gill, P. M. W.; Johnson, B.; Chen, W.; Wong, M. W.; Gonzalez, C.; Pople, J. A. *Gaussian*, Revision C.02; Gaussian, Inc.: Wallingford, CT, 2004.
(34) Peng, Y. Q.; Song, G. H.; Qian, X. H. *Synth. Commun.* **2001**, *31*, 1927–1931.
(35) Lippert, E. *Z. Naturforsch.* **1955**, *10a*, 541.
(36) Hadad, C. M.; Foresman, J. B.; Wiberg, K. B. *J. Phys. Chem.* **1993**, *97*, 4293–4312.
(37) Jodicke, C. J.; Luthi, H. P. *J. Am. Chem. Soc.* **2003**, *125*, 252–264.
(38) Dobkowski, J.; Wojcik, J.; Kozminski, W.; Kolos, R.; Waluk, J.; Michi, J. *J. Am. Chem. Soc.* **2002**, *124*, 2406–2407.
(39) Becke, A. D. *Phys. Rev. A* **1988**, *38*, 3098–3100.
(40) Lee, C. T.; Yang, W. T.; Parr, R. G. *Phys. Rev. B* **1988**, *37*, 785–789.
(41) Vyas, S.; Hadad, C. M.; Modarelli, D. A. *J. Phys. Chem. A* **2008**, *112*, 6533–6549.
(42) Wang, J.; Kubicki, J.; Burdzinski, G.; Hackett, J. C.; Gustafson, T. L.; Hadad, C. M.; Platz, M. S. *J. Org. Chem.* **2007**, *72*, 7581–7586.
(43) Burdzinski, G.; Hackett, J. C.; Wang, J.; Gustafson, T. L.; Hadad, C. M.; Platz, M. S. *J. Am. Chem. Soc.* **2006**, *128*, 13402–13411.
(44) Burdzinski, G. T.; Gustafson, T. L.; Hackett, J. C.; Hadad, C. M.; Platz, M. S. *J. Am. Chem. Soc.* **2005**, *127*, 13764–13765.
(45) Dreuw, A.; Head-Gordon, M. *J. Am. Chem. Soc.* **2004**, *126*, 4007–4016.

JP901982R